

Chaotic thermal convection of couple-stress fluid layer

G. C. Layek · N. C. Pati

Received: 27 March 2017 / Accepted: 30 October 2017 / Published online: 13 November 2017
© Springer Science+Business Media B.V., part of Springer Nature 2017

Abstract In this work we study the pattern of bifurcations and intermittent-chaos of non-Newtonian couple-stress shallow fluid layer subject to heating from below. The couple-stress parameter delays onset of convection, synchronizes chaotic behavior, and decreases the heat transfer. Some global aspects of the dynamics such as homoclinic bifurcations and transition to chaos are explored. The effects of particle size on the intermittent-chaos regime at particular normalized Rayleigh number, say $r = 166.1$, are investigated. With the increase in couple-stress parameter, the present Lorenz-like system synchronizes to a steady state via a series of periodic solutions interspersed with intervals of chaotic behaviors.

Keywords Couple-stress fluid convection · Hopf bifurcation · Homoclinic explosion · Intermittent-chaos · Synchronization

List of symbols

\mathbf{V}	Velocity vector of the couple-stress fluid
T	Temperature field
T_0	Constant temperature at the lower surface
ΔT	Temperature difference of two surfaces
p	Fluid pressure

t, τ	Time
g	Acceleration due to gravity
h	Depth of the fluid layer
μ	Viscosity of the fluid
μ'	Couple-stress viscosity
κ	Thermal diffusion coefficient
ρ	Density of the fluid
ρ_0	Reference density of the fluid
$\hat{\mathbf{k}}$	Unit vector along z -axis
α	Thermal expansion coefficient
ψ	Stream function
θ	Temperature deviation from conduction state temperature
Ra	Thermal Rayleigh number
σ	Prandtl number
c_s	Couple-stress parameter
k	Wave number
r	Normalized Rayleigh number
b	A geometrical parameter ($0 < b < 4$)
l_1	First Lyapunov quantity

1 Introduction

Investigation on the pattern of convection is very important for understanding underlying mechanism of chaotic evolution and its intermittent behavior. Over several decades thermal convection for Newtonian fluids has been extensively studied and focused mainly on the stability of the fluid layer at the onset of convection [1, 2]. A new direction of research in this field has

G. C. Layek (✉) · N. C. Pati
Department of Mathematics, The University of Burdwan,
Burdwan, West Bengal 713104, India
e-mail: gclayek@math.buruniv.ac.in

been emerged after the pioneering work of Lorenz [3] who used the Rayleigh–Bénard convection problem to model equations for weather forecasting. He showed that depending upon the Rayleigh number, the dimensionless ratio of the destabilizing buoyancy force to the stabilizing viscous force, the low-dimensional system exhibits random, aperiodic behaviors. The system undergoes a sequence of local and global bifurcations at the transitional regime.

The understanding of convection patterns, bifurcations, onset of chaotic motion and its control depending upon material parameters of non-Newtonian fluids is important for applications in science and technology. Among available non-Newtonian fluid models, the couple-stress fluid model is very simple and easy for analysis. This kind of fluid is realistic in different aspects. The couple-stress and also micropolar fluids have widespread applications in medical and engineering sciences such as lubrication technology of loaded bearings [4–8], peristaltic transport of bio-fluids in conduits [9–12], blood flow through stenotic arteries [13, 14], extrusion of polymer fluids (see Refs. [15–17] for micropolar fluids), and cooling of metallic plate in a bath. The effects of couple-stresses on fluid flows were extensively studied by Stokes [18] in different geometries. The main feature of fluid couple-stresses is to introduce size-dependent effects on flows based on the material constant and dynamic viscosity, which are not present in classical viscous fluid models.

The stability of a layer of couple-stress fluid heated from below was first studied by Ahmadi [19]. Using linear stability theory, Banyal [20] derived a necessary condition for the onset of stationary convection. A global nonlinear stability analysis for thermoconvection of a couple-stress fluid has been studied by Sunil et al. [21]. They showed that the critical Rayleigh numbers at the onset of convection for both linear and nonlinear stability analysis are exactly the same and the couple-stress fluid is thermally more stable than the ordinary fluid. Recently, Jawdat et al. [22] studied numerically the effects of couple-stresses on chaotic convection. The convection of couple-stress fluid is delayed with increase in particle size in the fluid. At the onset of convection there is a direct proportion between the Rayleigh number and the couple-stress parameter (square of the dimensionless ratio of the particle size to the depth of the fluid layer).

The motivation of the present study is to focus the effects of particle size on convection and transition to

chaos of couple-stress fluids subject to heating from below. This will be useful in understanding engineering transports such as heat transfer in fluids with long-chain molecules, melting and solidification of liquid crystals, polymeric suspensions, and lubrication technology under the framework of microcontinuum hypothesis which enables to assume each macrovolume element to contain a microstructure, allowing polar effects such as the presence of couple-stresses and body couple.

We explore the effects of particle size on the thermoconvective motion of a horizontal couple-stress fluid layer by employing a low-dimensional approach. This leads to three-dimensional Lorenz-like model equations with four control parameters, namely the Prandtl number σ , the normalized Rayleigh number r , the modified couple-stress parameter c , and a geometrical parameter b . The effects of the couple-stress parameter on the stability, bifurcations, transition to chaos, and intermittent-chaos are investigated. The first Lyapunov quantity determines the stability of the bifurcating periodic orbit emerging via the Hopf bifurcation. How the system reaches the convection-less state with increasing values of couple-stress parameter is shown graphically and analyzed. Analysis reveals that the synchronization of chaos to a steady state takes place through a series of periodic motions interspersed with chaotic behavior and non-stable limit cycle.

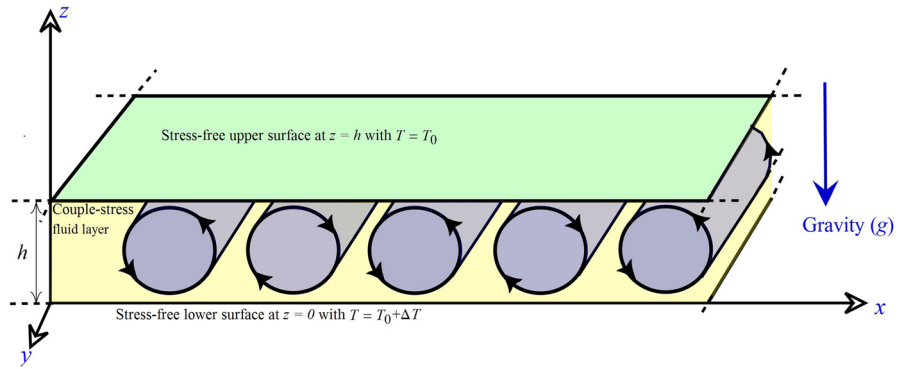
2 Convection model for couple-stress fluid

We consider gravity-driven thermal convection of a shallow, horizontally unbounded layer of an incompressible couple-stress fluid of depth h confined between two thermally conducting stress-free parallel planes subject to heating of the lower plane. A Cartesian coordinate system (x, y, z) is adopted with x -axis along the lower surface and z -axis vertically upward. Let $T_0 + \Delta T$ and T_0 be the temperature on the lower and upper surfaces, respectively. A schematic diagram of the flow domain with boundary conditions and other relevant thermo-physical parameters with clockwise and anticlockwise convection rolls is displayed in Fig. 1.

Then, the relevant hydrodynamic motion and heat transfer equations are written as [1, 18]

$$\rho_0 \frac{d\mathbf{V}}{dt} = -\nabla p + (\mu - \mu' \nabla^2) \nabla^2 \mathbf{V} - \rho g \hat{\mathbf{k}}, \quad (1)$$

Fig. 1 A physical sketch of thermo-fluid convection problem in a shallow fluid layer of depth h depicting convective rolls. The upper and lower boundaries are held at an isothermal temperatures T_0 and $T_0 + \Delta T$, respectively



$$\frac{dT}{dt} = \kappa \nabla^2 T, \tag{2}$$

where $d/dt \equiv \partial/\partial t + (\mathbf{V} \cdot \nabla)$. By adopting the Boussinesq approximation, the density variation in the buoyancy term is taken as $\rho = \rho_0 [1 - \alpha(T - T_0)]$, and the incompressibility condition is $\nabla \cdot \mathbf{V} = 0$.

Taking vector curl of (1) the pressure term is dropped out. In two-dimensional case all flow variables become independent of the y coordinate. Then, the velocity vector can be expressed in terms of stream function $\psi(x, z, t)$ as $\mathbf{V} = (-\partial\psi/\partial z, 0, \partial\psi/\partial x)$. Introducing the layer depth h as the length scale, h^2/κ as the time scale and ΔT as the temperature scale, the evolution equations for the perturbation field to the steady state of Eqs. (1) and (2) are written in dimensionless form as

$$\frac{\partial}{\partial t} (\nabla^2 \psi) + \frac{\partial (\nabla^2 \psi, \psi)}{\partial(z, x)} = \sigma (1 - c_s \nabla^2) \nabla^4 \psi + \sigma Ra \frac{\partial \theta}{\partial x}, \tag{3}$$

$$\frac{\partial \theta}{\partial t} + \frac{\partial (\theta, \psi)}{\partial(z, x)} = \frac{\partial \psi}{\partial x} + \nabla^2 \theta, \tag{4}$$

where θ represents the (dimensionless) temperature deviation from the conducting state temperature and $\frac{\partial(f_1, f_2)}{\partial(z, x)}$ denotes $\left(\frac{\partial f_1}{\partial z} \frac{\partial f_2}{\partial x} - \frac{\partial f_1}{\partial x} \frac{\partial f_2}{\partial z} \right)$ for arbitrary f_1 and f_2 .

In the above equations, the dimensionless parameters are $\sigma = \mu/(\rho_0 \kappa)$ the Prandtl number, $Ra = \rho_0 g \alpha \Delta T h^3 / (\kappa \mu)$ the Rayleigh number, and the couple-stress parameter $c_s = a^2$, where $a = d/h$ and $d = (\mu'/\mu)^{1/2}$. The quantity d has the dimension of length and therefore can be associated with the molecular length scale of the couple-stress fluid. The dimensionless quantity a represents the ratio of the particle size to the depth of the fluid layer. Thus, for a particular fluid layer depth, the effects of couple-stresses increase with the particle size in the fluid. However, the molecular size and flow length scale must have some limitations and do not exceed the limitation of continuum theory for constitutive equations.

Now we shall precise the boundary conditions of this thermo-convective problem. Since the two bounding surfaces are stress-free, the boundary conditions for the dimensionless stream function ψ are written as

$$\psi = \frac{\partial^2 \psi}{\partial z^2} = 0 \quad \text{on} \quad z = 0, 1. \tag{5}$$

In addition, since the temperature is fixed on the boundaries, we have

$$\theta = 0 \quad \text{on} \quad z = 0, 1. \tag{6}$$

For spatiotemporal evolution, the variables ψ and θ are expanded in Fourier series of x and z , following Lorenz [3], as

$$\left. \begin{aligned} \psi(x, z, t) &= \frac{\sqrt{2}\Lambda}{\pi k} X(\tau) \sin(kx) \sin(\pi z) \\ \theta(x, z, t) &= \frac{\sqrt{2}\Lambda^3}{\pi k^2 Ra} Y(\tau) \cos(kx) \sin(\pi z) \\ &\quad - \frac{\Lambda^3}{\pi k^2 Ra} Z(\tau) \sin(2\pi z) \end{aligned} \right\} \tag{7}$$

where $\Lambda = \pi^2 + k^2$, k being the horizontal wavenumber, and $\tau = \Lambda t$ is the rescaled time variable. Obviously, the boundary conditions (5) and (6) are satisfied. Projecting Eqs. (3) and (4) onto the modes of Eq. (7), we obtain the following three-dimensional nonlinear system

$$\left. \begin{aligned} \dot{X} &= \sigma(Y - cX) \\ \dot{Y} &= rX - Y - XZ \\ \dot{Z} &= XY - bZ \end{aligned} \right\} \tag{8}$$

where dot denotes derivative with respect to dimensionless time τ , $r = Ra/Ra_c$ is the normalized Rayleigh number with $Ra_c = \Lambda^3/k^2$, $c = 1 + \Lambda c_s$ the modified couple-stress parameter, and $b = 4\pi^2/\Lambda$ a geometrical parameter lying in $0 < b < 4$. In Eq. (8), the mode X represents the velocity field and the other two modes Y and Z describe, respectively, the change in the temperature along the horizontal and vertical directions. In the absence of fluid couple-stresses (i.e., $c_s = 0$), Eq. (8) reduces to Lorenz system [3] corresponding to Newtonian fluid. Note that very recently Layek and Pati [23] derived a five-dimensional generalized Lorenz system for hyperbolic heat propagation in Newtonian fluid media.

The present nonlinear system (8) possesses two important properties. First, it is invariant under the transformation $(X, Y, Z) \rightarrow (-X, -Y, Z)$. Second, the flow divergence $\nabla \cdot (\dot{X}, \dot{Y}, \dot{Z}) = -(1 + b + c\sigma)$ is negative always. So, the system is dissipative and its solutions are bounded in the phase space.

3 Bifurcations from the steady solutions

In this section, we study the stability and bifurcations of the system (8) at its equilibrium or fixed points. The equilibrium points (or constant solutions or steady solutions) of (8) can be obtained by solving the equations $\dot{X} = 0, \dot{Y} = 0, \dot{Z} = 0$, i.e., $Y = cX, rX - Y - XZ = 0, XY = bZ$, which, after simplification, give a trivial solution $E_0 = (0, 0, 0)$ and two symmetric non-trivial equilibrium solutions $E_{\pm} = (\pm\sqrt{b(r-c)}/c, \pm\sqrt{bc(r-c)}, r-c)$. Physically, the trivial solution E_0 represents the conducting state (state of no convection) of the couple-stress fluid layer, while the non-trivial solutions E_{\pm} correspond to the steady convective state of the fluid layer.

The stability of the system (8) at the trivial equilibrium point E_0 can be obtained by linearizing it about E_0 and taking trial solutions of the form $\exp(s\tau)$. This gives the characteristic equation

$$\det \begin{pmatrix} s + c\sigma & -\sigma & 0 \\ -r & s + 1 & 0 \\ 0 & 0 & s + b \end{pmatrix} = 0. \tag{9}$$

From Eq. (9), we have one characteristic root (eigenvalue) as $s = -b$ and the other two eigenvalues satisfy

$$s^2 + (1 + c\sigma)s + \sigma(c - r) = 0. \tag{10}$$

The stability of E_0 can be determined by the signs of the eigenvalues. It is stable if all of the three eigenvalues have negative real part; it is unstable if the real part of at least one eigenvalue is positive. The system undergoes a bifurcation at E_0 if it has either a zero eigenvalue or a pair of purely imaginary eigenvalues. Physically, a bifurcation in the thermo-convective motion corresponds to an onset of instability in the fluid layer.

Since b is positive, the eigenvalue $s = -b$ is negative always and so the onset of instability in the static solution E_0 depends on the roots of Eq. (10) only. Setting $s = 0$ in (10), an exchange of stability (onset of stationary convection) takes place at the normalized Rayleigh number $r_p = c$ and it becomes $r_p = 1$ for Newtonian fluids ($c_s = 0$). In this work, the parameters k and σ are taken as $\pi/\sqrt{2}$ and 10, respectively. Then, $b = 8/3$ and $r_p = c = 1 + (3/2)\pi^2 c_s$. Since the roots of (10) are always real, the system cannot exhibit overstable motion (oscillatory onset of convection). So the onset of instability sets in only via stationary modes (pitchfork bifurcation), when r increases r_p . In the neighborhood of the bifurcation point r_p the system has three steady solutions. One is the static solution E_0 which is always unstable for $r > r_p$, and the other two are the finite amplitude convective solutions E_{\pm} existing only when $r > r_p$. Using normal form theory [24,25], the non-trivial solutions are supercritical (stable) in the neighborhood of the pitchfork bifurcation point.

For stability of the convective solutions E_{\pm} beyond r_p , we consider only the positive solutions since they are symmetric in nature. For linear stability of E_+ , we first apply a small perturbation to E_+ as follows:

$$x_2 = X - x_0, \quad y_2 = Y - cx_0, \quad z_2 = Z - (r - c), \tag{11}$$

where $x_0 = \sqrt{b(r-c)}/c$. Using (11) into Eq. (8), the perturbation equations are obtained as

$$\left. \begin{aligned} \dot{x}_2 &= \sigma y_2 - c\sigma x_2 \\ \dot{y}_2 &= cx_2 - y_2 - x_0 z_2 - x_2 z_2 \\ \dot{z}_2 &= cx_0 x_2 + x_0 y_2 - bz_2 + x_2 y_2 \end{aligned} \right\} \tag{12}$$

with the origin as an equilibrium point. Linearizing (12) about the origin and assuming exponential evolution in

time for the perturbation admits the following cubic equation for the eigenvalues

$$s^3 + a_1s^2 + a_2s + a_3 = 0, \tag{13}$$

where $a_1 = 1 + b + c\sigma$, $a_2 = br/c + \sigma bc$, and $a_3 = 2b\sigma(r - c)$.

Following Routh–Hurwitz stability criteria, the necessary (but not sufficient) condition [26] for linear stability of E_+ is that the quantities a_1 , a_2 , a_3 , and f are all positive, where $f = a_1a_2 - a_3$. Under this condition, the eigenvalues from Eq. (13) have negative real part. The instability sets in when at least one eigenvalue crosses the origin (for real eigenvalues) or a pair of eigenvalues cross the imaginary axis (for complex eigenvalues) to the positive half-plane. In the former case, the coefficient a_3 must change its sign first, whereas for the latter case the quantity f changes its sign first [26].

Thus, depending on the quantities a_3 and f one can find the critical Rayleigh number at the onset of instability in the convective solutions. Since $r > c$ for the convective solutions, we have $a_3 > 0$ always. So, the possibility of existence of instability now depends on f alone. In this case, the system undergoes a Hopf bifurcation in the neighborhood of E_+ provided the coefficients a_j ($j = 1, 2, 3$) satisfy the relation $a_1a_2 - a_3 = 0$, which gives the critical normalized Rayleigh number at the onset of the Hopf bifurcation as $r_h = \sigma c^2(3 + b + c\sigma)/(c\sigma - b - 1)$, provided $\sigma > (1 + b)/c$. At the Hopf bifurcation point r_h , the linearized system has a pair of purely imaginary eigenvalues $s_{\pm} = \pm i\omega$ ($i = \sqrt{-1}$) with the frequency of oscillation $\omega = \sqrt{\frac{2\sigma bc(1+c\sigma)}{c\sigma - b - 1}}$. The third eigenvalue $s_3 = -(1 + b + c\sigma)$ is real and negative. Appearance of Hopf bifurcation at $r = r_h$ indicates that an infinitesimal perturbation to the steady convective state of the fluid layer may result in oscillatory motion in the system.

4 Sub- and supercritical Hopf bifurcations

By knowing how the solution E_+ loses its stability via Hopf bifurcation as r is increased through the critical value r_h , one can categorize the Hopf bifurcation into two types, namely supercritical and subcritical Hopf bifurcations. By supercritical Hopf bifurcation, it gen-

erally means that the bifurcation destabilizes the equilibrium point E_+ to a unique small-amplitude stable limit cycle whose periodic orbit can be detected numerically. On the other hand, for subcritical Hopf bifurcation no such small-amplitude limit cycle will be created after the bifurcation. In this case, E_+ loses its stability by absorbing a saddle limit cycle. A quantity that determines the type of the Hopf bifurcation is the first Lyapunov quantity, usually denoted by l_1 (see Kuznetsov [27] for details). The Hopf bifurcation is supercritical if $l_1 < 0$ and subcritical when $l_1 > 0$. For $l_1 = 0$, we have codimension-2 degenerate Hopf bifurcation.

In order to determine whether the Hopf bifurcation is sub- or supercritical we follow the technique described in Hassard et al. [28] based on normal form theory. First, we fix the parameter r at the Hopf bifurcation point r_h . The eigenvectors corresponding to the eigenvalues $s_+ = i\omega$ and $s_3 = -(1 + b + c\sigma)$ are obtained as

$$e_+ = \begin{pmatrix} 1 \\ c + i\frac{\omega}{\sigma} \\ \frac{\omega^2 - i(1+c\sigma)\omega}{\sigma x_0} \end{pmatrix} \quad \text{and} \quad e_3 = \begin{pmatrix} -\frac{\sigma}{1+b} \\ 1 \\ \frac{b(1+b+c\sigma)}{(1+b)x_0} \end{pmatrix},$$

respectively, where $x_0 = \sqrt{\frac{b(1+c\sigma)(1+b+c\sigma)}{(c\sigma - b - 1)}}$.

Let us now apply the transformation $(x_2, y_2, z_2)' = \mathbf{A}(x_1, y_1, z_1)'$ to Eq. (12), where ‘ $'$ ’ denotes transposition and the matrix \mathbf{A} is given by

$$\mathbf{A} = (\text{Re } e_+, -\text{Im } e_+, e_3) = \begin{pmatrix} 1 & 0 & -\frac{\sigma}{1+b} \\ c & -\frac{\omega}{\sigma} & 1 \\ \frac{\omega^2}{\sigma x_0} & \frac{(1+c\sigma)\omega}{\sigma x_0} & \frac{b(1+b+c\sigma)}{(1+b)x_0} \end{pmatrix}.$$

This gives the following normalized system

$$\left. \begin{aligned} \dot{x}_1 &= -\omega y_1 + F_1(x_1, y_1, z_1) \\ \dot{y}_1 &= \omega x_1 + F_2(x_1, y_1, z_1) \\ \dot{z}_1 &= -(1 + b + c\sigma)z_1 + F_3(x_1, y_1, z_1) \end{aligned} \right\} \tag{14}$$

The functions F_1 , F_2 , and F_3 in (14) are given by

$$\begin{aligned} F_1(x_1, y_1, z_1) &= \frac{lx_0}{1+b} P(x_1, y_1, z_1) \\ &\quad - \frac{l(1+c\sigma)}{x_0(1+b)^2} Q(x_1, y_1, z_1), \\ F_2(x_1, y_1, z_1) &= \frac{lx_0(1+b+c\sigma)}{\omega(1+b)} P(x_1, y_1, z_1) \\ &\quad + l \frac{\omega^2 + b(1+b+c\sigma)}{x_0\omega(1+b)^2} Q(x_1, y_1, z_1), \end{aligned}$$

$$F_3(x_1, y_1, z_1) = \frac{lx_0}{\sigma} P(x_1, y_1, z_1) - \frac{l(1+c\sigma)}{(1+b)\sigma x_0} Q(x_1, y_1, z_1),$$

where P , Q , and l are as follows:

$$P(x_1, y_1, z_1) = \{(1+b)x_1 - \sigma z_1\} \\ (c\sigma x_1 - \omega y_1 + \sigma z_1), \\ Q(x_1, y_1, z_1) = \{(1+b)x_1 - \sigma z_1\} \\ \left\{ (1+b)\omega^2 x_1 + \omega(1+b)(1+c\sigma)y_1 \right. \\ \left. + b\sigma(1+b+c\sigma)z_1 \right\}, \\ \text{and } l = 1/\left(\omega^2 + (1+b+c\sigma)^2\right).$$

The normal form theory requires the evaluation of the following quantities for Eq. (14),

$$g_{11} = \frac{1}{4} \left[\frac{\partial^2 F_1}{\partial x_1^2} + \frac{\partial^2 F_1}{\partial y_1^2} + i \left(\frac{\partial^2 F_2}{\partial x_1^2} + \frac{\partial^2 F_2}{\partial y_1^2} \right) \right] \\ = \frac{l}{2} (\alpha_1 + i\beta_1), \\ g_{02} = \frac{1}{4} \left[\frac{\partial^2 F_1}{\partial x_1^2} - \frac{\partial^2 F_1}{\partial y_1^2} - 2 \frac{\partial^2 F_2}{\partial x_1 \partial y_1} \right. \\ \left. + i \left(\frac{\partial^2 F_2}{\partial x_1^2} - \frac{\partial^2 F_2}{\partial y_1^2} + 2 \frac{\partial^2 F_1}{\partial x_1 \partial y_1} \right) \right] \\ = \frac{l}{2} (\alpha_2 + i\beta_2), \\ g_{20} = \frac{1}{4} \left[\frac{\partial^2 F_1}{\partial x_1^2} - \frac{\partial^2 F_1}{\partial y_1^2} + 2 \frac{\partial^2 F_2}{\partial x_1 \partial y_1} \right. \\ \left. + i \left(\frac{\partial^2 F_2}{\partial x_1^2} - \frac{\partial^2 F_2}{\partial y_1^2} - 2 \frac{\partial^2 F_1}{\partial x_1 \partial y_1} \right) \right] \\ = \frac{l}{2} (\alpha_3 + i\beta_3), \\ G_{21} = \frac{1}{8} \left[\frac{\partial^3 F_1}{\partial x_1^3} + \frac{\partial^3 F_1}{\partial x_1 \partial y_1^2} + \frac{\partial^3 F_2}{\partial x_1^2 \partial y_1} + \frac{\partial^3 F_2}{\partial y_1^3} \right. \\ \left. + i \left(\frac{\partial^3 F_2}{\partial x_1^3} + \frac{\partial^3 F_2}{\partial x_1 \partial y_1^2} - \frac{\partial^3 F_1}{\partial x_1^2 \partial y_1} - \frac{\partial^3 F_1}{\partial y_1^3} \right) \right] \\ = 0, \\ h_{11} = \frac{1}{4} \left(\frac{\partial^2 F_3}{\partial x_1^2} + \frac{\partial^2 F_3}{\partial y_1^2} \right)$$

$$= \frac{l}{2} \alpha_4,$$

$$h_{20} = \frac{1}{4} \left(\frac{\partial^2 F_3}{\partial x_1^2} - \frac{\partial^2 F_3}{\partial y_1^2} - 2i \frac{\partial^2 F_3}{\partial x_1 \partial y_1} \right)$$

$$= \frac{l}{2} (\alpha_4 + i\beta_4),$$

$$G_{110} = \frac{1}{2} \left[\frac{\partial^2 F_1}{\partial x_1 \partial z_1} + \frac{\partial^2 F_2}{\partial y_1 \partial z_1} \right. \\ \left. + i \left(\frac{\partial^2 F_2}{\partial x_1 \partial z_1} - \frac{\partial^2 F_1}{\partial y_1 \partial z_1} \right) \right] = \frac{l}{2} (\alpha_5 + i\beta_5),$$

$$G_{101} = \frac{1}{2} \left[\frac{\partial^2 F_1}{\partial x_1 \partial z_1} - \frac{\partial^2 F_2}{\partial y_1 \partial z_1} \right. \\ \left. + i \left(\frac{\partial^2 F_2}{\partial x_1 \partial z_1} + \frac{\partial^2 F_1}{\partial y_1 \partial z_1} \right) \right] = \frac{l}{2} (\alpha_6 + i\beta_6),$$

where $\alpha_j, \beta_j, j = 1, 2, \dots, 6$ are given below

$$\alpha_1 = x_0 c \sigma - (1+c\sigma)\omega^2/x_0, \\ \alpha_2 = \alpha_1 - (1+c\sigma)(\omega^2 + b(1+b+c\sigma))/x_0 \\ + x_0(1+b+c\sigma), \\ \alpha_3 = \alpha_1 + (1+c\sigma)(\omega^2 + b(1+b+c\sigma))/x_0 \\ - x_0(1+b+c\sigma), \\ \alpha_4 = x_0 c(1+b) - \omega^2(1+b)(1+c\sigma)/(\sigma x_0), \\ \alpha_5 = 2x_0 \sigma - 2b\sigma(1+c\sigma)(1+b+c\sigma)/(x_0(1+b)), \\ \alpha_6 = 2\sigma(1+c\sigma)\omega^2/(x_0(1+b)) \\ - 2x_0 c \sigma^2/(1+b),$$

and

$$\beta_1 = x_0 c \sigma(1+b+c\sigma)/\omega \\ + \omega(\omega^2 + b(1+b+c\sigma))/x_0, \\ \beta_2 = \beta_1 - \omega(1+c\sigma)^2/x_0 - x_0 \omega, \\ \beta_3 = \beta_1 + \omega(1+c\sigma)^2/x_0 + x_0 \omega, \\ \beta_4 = \omega(1+b)(1+c\sigma)^2/(\sigma x_0) + x_0 \omega(1+b)/\sigma, \\ \beta_5 = -\frac{x_0 \sigma(c\sigma + b + 1)(c\sigma - b - 1)}{\omega(1+b)} \\ - \frac{\sigma(\omega^4 - b^2(1+b+c\sigma)^2)}{x_0 \omega(1+b)} \\ - \frac{x_0 \omega \sigma}{1+b} - \frac{\sigma \omega(1+c\sigma)^2}{x_0(1+b)},$$

$$\beta_6 = -\frac{x_0\sigma(c\sigma + b + 1)(c\sigma - b - 1)}{\omega(1 + b)} - \frac{\sigma(\omega^4 - b^2(1 + b + c\sigma)^2)}{x_0\omega(1 + b)} + \frac{x_0\omega\sigma}{1 + b} + \frac{\sigma\omega(1 + c\sigma)^2}{x_0(1 + b)}.$$

Now solving the equations $s_3w_{11} = -h_{11}$ and $(s_3 - 2i\omega)w_{20} = -h_{20}$, we have

$$w_{11} = \frac{l}{2(1 + b + c\sigma)}\alpha_4,$$

and $w_{20} = \frac{l}{2\{(1 + b + c\sigma)^2 + 4\omega^2\}}(\alpha_7 + i\beta_7),$

where $\alpha_7 = (1 + b + c\sigma)\alpha_4 + 2\omega\beta_4$ and $\beta_7 = (1 + b + c\sigma)\beta_4 - 2\omega\alpha_4$. Using the above quantities, we obtain

$$l_1(c_s) = \frac{\text{Re } C_1(r_h)}{\omega} = \frac{l^2}{8} \left[\frac{2(4\omega^2 + (1 + b + c\sigma)^2)\alpha_4\alpha_5 + (1 + b + c\sigma)^2(\alpha_4\alpha_6 - \beta_4\beta_6) + 2\omega(1 + b + c\sigma)(\beta_4\alpha_6 + \alpha_4\beta_6)}{\omega(1 + b + c\sigma)(4\omega^2 + (1 + b + c\sigma)^2)} - \frac{\alpha_1\beta_3 + \beta_1\alpha_3}{\omega^2} \right]. \tag{15}$$

$$g_{21} = G_{21} + 2G_{110}w_{11} + G_{101}w_{20} = \frac{l^2}{4(1 + b + c\sigma)\{(1 + b + c\sigma)^2 + 4\omega^2\}} \times (\alpha_8 + i\beta_8),$$

where

$$\alpha_8 = 2\{(1 + b + c\sigma)^2 + 4\omega^2\} \alpha_4\alpha_5 + (1 + b + c\sigma)(\alpha_6\alpha_7 - \beta_6\beta_7),$$

and $\beta_8 = 2\{(1 + b + c\sigma)^2 + 4\omega^2\} \alpha_4\beta_5 + (1 + b + c\sigma)(\alpha_6\beta_7 + \alpha_7\beta_6).$

Finally, we calculate

$$C_1(r_h) = \frac{i}{2\omega} \left(g_{20}g_{11} - 2|g_{11}|^2 - \frac{1}{3}|g_{02}|^2 \right) + \frac{g_{21}}{2} = \frac{l^2}{8} \left[\frac{\alpha_8}{(1 + b + c\sigma)(4\omega^2 + (1 + b + c\sigma)^2)} - \frac{\alpha_1\beta_3 + \beta_1\alpha_3}{\omega} + i \left\{ \frac{\alpha_1\alpha_3 - \beta_1\beta_3}{\omega} \right\} \right]$$

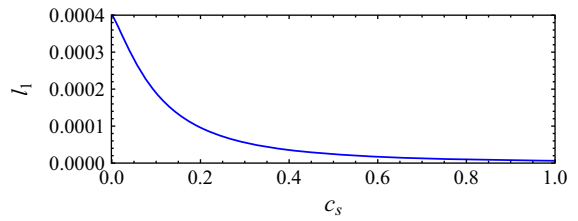


Fig. 2 Variation of the first Lyapunov quantity l_1 with the couple-stress parameter c_s

$$\left. \begin{aligned} & - 2(\alpha_1^2 + \beta_1^2) - \frac{\alpha_2^2 + \beta_2^2}{3} \\ & + \frac{\beta_8}{(1 + b + c\sigma)(4\omega^2 + (1 + b + c\sigma)^2)} \end{aligned} \right\}.$$

The nature of the Hopf bifurcation for the normalized system (14) can be determined by the first Lyapunov quantity [27]

The stability of the Hopf bifurcation depends on the sign of l_1 . The determination of the sign of l_1 from (15) is very difficult analytically because of its complicated expression. So numerical simulations are desirable for the sign of l_1 over the parameter range. The variation of l_1 with the couple-stress parameter c_s is displayed graphically in Fig. 2. As shown, the value of l_1 decreases with the increase in couple-stress parameter c_s , but it never reaches zero value. Hence, the Hopf bifurcation at $r = r_h$ is always subcritical type, like in Lorenz system. However, as c_s is increased, the hardness of the stability boundary at $r = r_h$ gradually decreases (hard to soft bifurcations). The quantity r_h is increasing nonlinearly with couple-stress parameter c_s . So it delays the transition to chaotic convection.

5 Nonlinear behaviors: homoclinic explosion and the transition to chaos

So far we have discussed the effects of couple-stress parameter on the stability of the steady solutions and

Fig. 3 The oscillatory decaying phase trajectories (projected onto the X - Y plane) to the equilibrium points E_{\pm} for the parameters values: **a** $r = 35$, $c_s = 0.1$ and **b** $r = 35$, $c_s = 0.3$

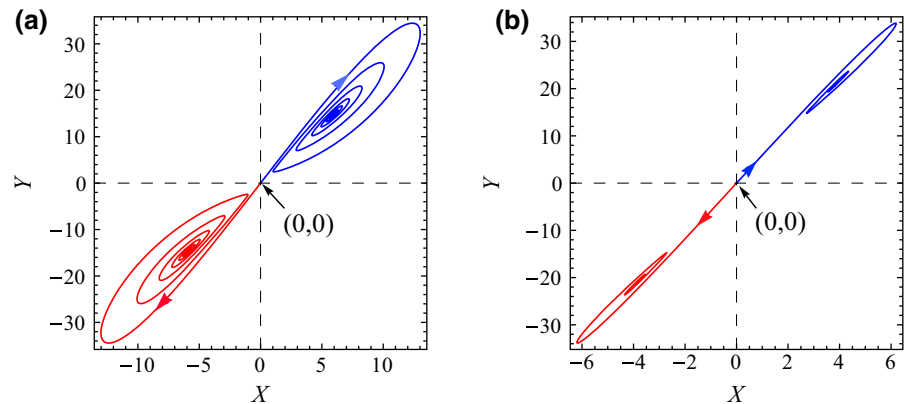
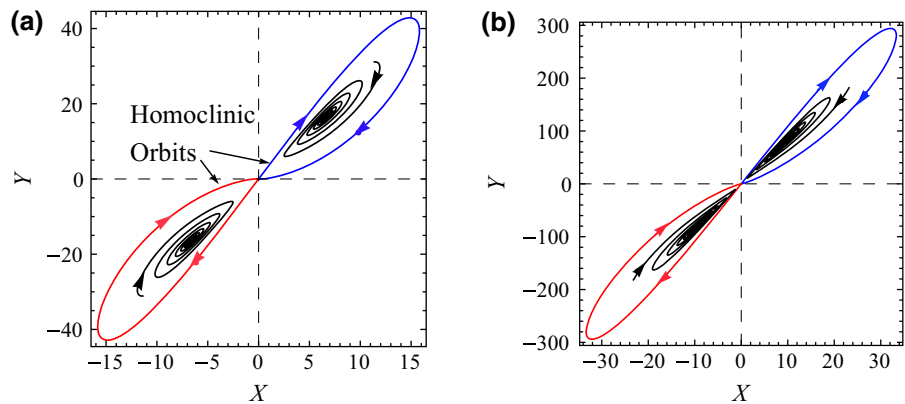


Fig. 4 Existence of homoclinic orbits for **a** $r = 43.4092$, $c_s = 0.1$, and **b** $r = 295.755$, $c_s = 0.5$



local bifurcation scenarios for the Lorenz-like system (8). In this section, we explore some global aspects of the dynamics, viz. homoclinic bifurcation and the transition to chaos. In nonlinear dynamics, a homoclinic bifurcation and the corresponding changes in dynamics are crucially important. This global behavior leads to change in deterministic dynamics from being robust and predictable to being chaotic [29].

Consider the range of the normalized Rayleigh number r between r_p and r_h . Within this range, one can find a point (say r_s) beyond which all the trajectories started near the origin on its unstable manifold decay spirally toward one of the equilibrium points E_{\pm} . The trajectories on the positive half-space decay toward the point E_+ , while those on the negative half-space decay toward E_- (Fig. 3 illustrates flow trajectories behaviors).

As r is increased, the amplitude of oscillation of the flow trajectories becomes larger and larger with r until it reaches a critical value, r_0 , beyond which the trajectories that attracted to E_+ now cross over this point and move toward the point E_- and vice versa.

An interesting feature is observed when r attains the critical value r_0 . At this point, the trajectories started near the origin on its unstable manifold attracted to its stable manifold, creating a closed orbit surrounding the point E_+ or E_- , which connects the origin with itself (see Fig. 4). Such an orbit is called a homoclinic orbit. The bifurcation associated with a homoclinic orbit at the origin for $r = r_0$ is known as the homoclinic bifurcation or ‘homoclinic explosion’ [30]. It is a global bifurcation at the origin that cannot be revealed by the linearization technique. Note that homoclinic bifurcations play a role where the transition to chaos occurs immediately for a critical value of the parameter (see Broer and Takens [31] and references therein). The values of r_0 at the onset of the homoclinic bifurcation are listed in Table 1 for increasing values of c_s . The critical value increases with the increase in c_s , resulting in the delay of homoclinic bifurcation of the system.

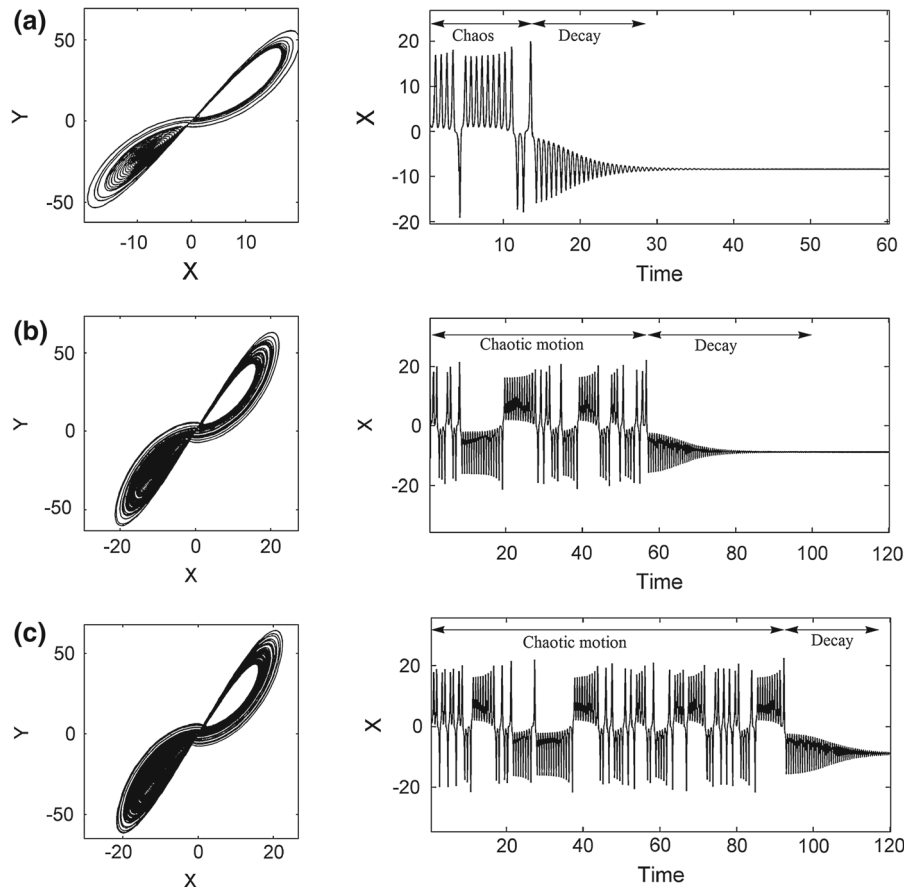
For r just above r_0 , the system has non-stable periodic orbit surrounding either of the points E_{\pm} in a strange invariant set created through the homoclinic

Table 1 Approximate values of r_0 for increasing couple-stress parameter c_s

c_s	r_0 (Critical value for homoclinic orbit)
0.0	13.926 (Lorenz system)
0.1	43.4092
0.2	87.102
0.3	143.98045
0.4	213.617
0.5	295.755
0.6	390.21273
0.7	496.855
0.8	615.576
0.9	746.2927
1.0	888.934

bifurcation. For r near r_0 , the periodic orbit is found to pass very close to the origin. But it moves away from the origin decreasing its period of oscillation with r .

Fig. 5 Phase portrait (on X - Y plane) (left) and time history (X vs. time τ) (right) of the solution of (8) for $c_s = 0.1$ at different reduced Rayleigh numbers **a** $r = 68$, **b** $r = 74$, **c** $r = 76$. As displayed, the time interval of random oscillation increases with r . After the chaotic oscillation, the flow trajectory decays spirally to the equilibrium point E_-



Eventually, it shrinks to the equilibrium point E_+ or E_- when r is increased to r_h .

For the flow trajectory beyond the critical value for homoclinic orbit, r_0 , we see that as r increases the trajectory wanders randomly around the non-trivial equilibrium points E_{\pm} , eventually decays to either of them. The average time interval of wandering is finite; it expands with r . Finally, the time interval tends to infinity when r attains another critical value $r_1 (< r_h)$. Figure 5a–c display the phase portrait on the X - Y plane and time history (X versus τ), which clearly indicate the chaotic and decaying behaviors for three different values of r at fixed value of c_s . For $r = r_1$, the trajectory of the strange attractor wanders chaotically around the points E_{\pm} . It takes infinitely large time to decay toward the equilibrium points. This phenomenon of chaotic wandering before the onset of the subcritical Hopf bifurcation was reported by Kaplan and Yorke [32] and by Yorke and Yorke [33], and they termed it as ‘preturbulence’ [32], or ‘metastable chaos’ [33].

Table 2 Approximate values of r_1 for increasing couple-stress parameter c_s

c_s	r_1 (Critical value for strange attractor)
0.0	24.06 (Lorenz system)
0.1	76.8407
0.2	153.45
0.3	263.04
0.4	380.95
0.5	544.41
0.6	742.698

The numerically computed values of r_1 (listed in Table 2) increase with the couple-stress parameter c_s , which clearly indicates the suppression effects of fluid couple-stresses on the chaotic evolution of the present system.

6 Intermittency, intermittent-chaos, and synchronization of couple-stress fluid convection

Intermittency is a typical route of chaos in deterministic nonlinear systems. It is characterized by long periods of regular motion interrupted by random, aperiodic short-duration bursts. These chaotic bursts become more frequent in course of time evolution [25, 34]. The intermittency phenomenon in the Lorenz system was first studied numerically by Pomeau and Manneville [35]. They showed that the Lorenz system exhibits an intermittent transition to chaos at the critical normalized Rayleigh

number $r_T \approx 166.06$. In this section, we investigate the effects of couple-stress parameter c_s on the dynamics of the intermittent-chaos at $r = 166.1 > r_T$.

We now focus our attention on the bifurcation diagram of the system. Figure 6 displays the bifurcation diagram representing the local extrema of Z in the post-transient solution of $Z(t)$ at $r = 166.1$ as a function of the couple-stress parameter c_s . The white stripes in the bifurcation diagram correspond to periodic windows.

In this connection we define Poincaré map which is useful for analyzing complex dynamics of nonlinear systems. There exists a map where each state $(\phi, \dot{\phi})$ is connected to the next state $P(\phi, \dot{\phi})$. In other way, whenever $\phi(t)$ is a solution of the system, one obtains $P(\phi(t_n), \dot{\phi}(t_n)) = (\phi(t_{n+1}), \dot{\phi}(t_{n+1}))$, $n = 0, 1, 2, \dots$. This map is called the Poincaré return map or period map or stroboscopic map. However, for construction of bifurcation diagram from Poincaré map the selection of appropriate Poincaré section is very important [30, 36].

It is clear from the bifurcation diagram that the sequence of events through which the chaotic motion at $c_s = 0$ synchronizes to a steady state as c_s is increased. In the broad spectrum of the chaotic regimes, there exist periodic motions of certain periods. The periods can be determined by using the Poincaré return map. Here all post-transient return maps are constructed on the plane $Z = 165$. The evolutions of the flow trajectories for intermittent-chaos (at $r = 166.1$) with increasing values of c_s are represented graphically in Figs. 7, 8, 10, 11, 12, and 13.

Fig. 6 Bifurcation diagram (Z vs. c_s) of the intermittent-chaos at the normalized Rayleigh number $r = 166.1$ representing the local extrema of Z in the post-transient solution of $Z(t)$ as a function of the couple-stress parameter c_s . The other parameters are fixed at $\sigma = 10$, $b = 8/3$. The white stripes correspond to the periodic windows

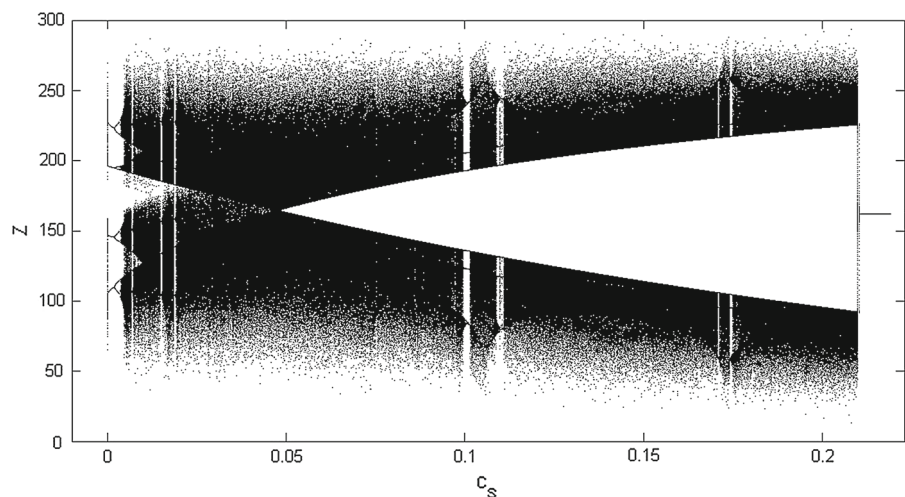


Fig. 7 Phase portrait of the intermittent-chaos(at $r = 166.1$) projected onto the X - Y plane (left) and the corresponding Poincaré map (right) for the couple-stress parameter: **a** $c_s = 0.0$, **b** $c_s = 0.001$

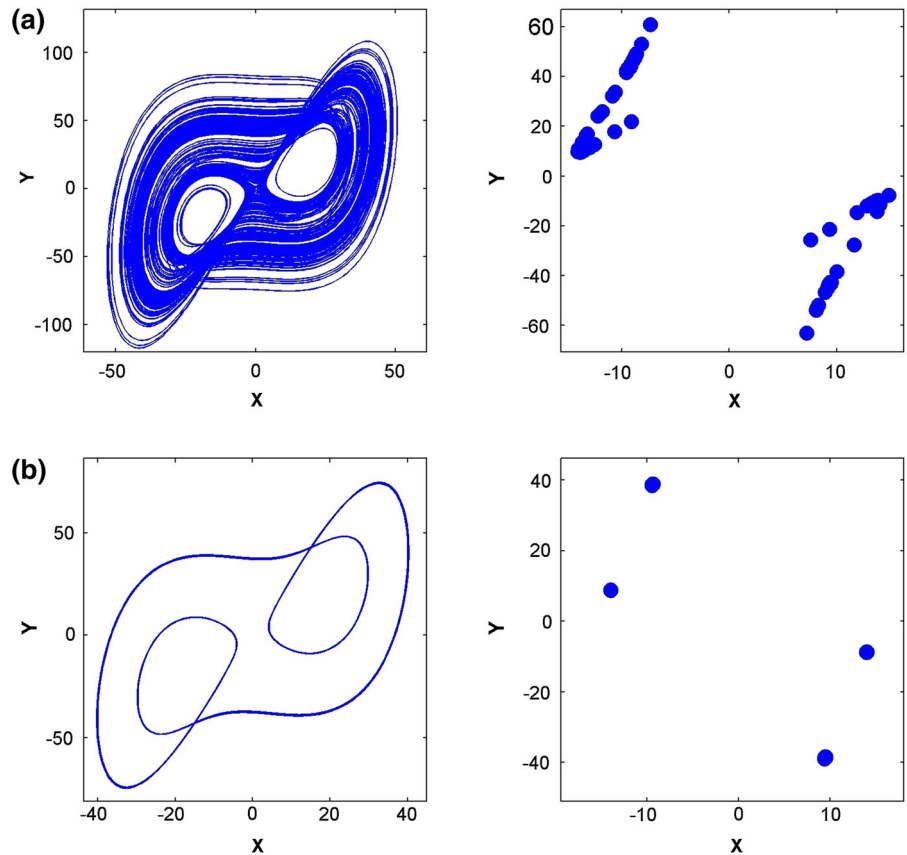


Figure 7a presents the Poincaré return map depicting intermittent-chaos at $r = 166.1$ and $c_s = 0$. As shown, two hooks appear on the Poincaré section. Actually, the hooks in the Poincaré map correspond to the contraction of nearby solution trajectories which causes one or more unstable periodic orbits to become stable. As a result, the system undergoes homoclinic explosion to a stable periodic orbit which can be detected numerically as c_s is increased (see Sparrow [30], Vadasz and Olek [36]). As expected, a periodic solution is obtained at $c_s = 0.001$ displayed in Fig. 7b, and the orbit is of period-4.

Above $c_s \approx 0.0036$, the solution becomes chaotic again. For $c_s = 0.005$, the chaotic attractor is displayed graphically in Fig. 8a. The chaotic solution can also be confirmed by calculating the Lyapunov exponents [37]. Being three-dimensional, the present nonlinear system has three Lyapunov exponents (LEs). A chaotic attractor of (8) is quantified by Lyapunov spectra with a positive Lyapunov exponent. For periodic/quasi-periodic attractors, the largest LE is zero. For fixed point attrac-

tors, all the three LEs are negative [37]. The variation of the two leading Lyapunov exponents, say $\lambda_{1,2}$, with the couple-stress parameter $c_s \in [0, 0.22]$, is displayed graphically in Fig. 9a. In this range of c_s , the Kaplan–Yorke dimension (or the Lyapunov dimension) can be easily calculated. This enables one to estimate the fractal dimension of the underlying attractor displayed in the figures. The Kaplan–Yorke dimension of an attractor of system (8) with Lyapunov exponents $\lambda_1 \geq \lambda_2 \geq \lambda_3$ is defined as $D_{KY} = m + \frac{\sum_{j=1}^m \lambda_j}{|\lambda_{m+1}|}$, where m is the largest positive integer such that $\sum_{j=1}^m \lambda_j \geq 0$ [38]. If no such positive integer m exists, then $D_{KY} = 0$. The variation of D_{KY} with c_s is presented graphically in Fig. 9b.

The two hooks in the return map (see Fig. 8a) indicate the existence of periodic orbits via homoclinic explosion. A period-8 periodic orbit is obtained at $c_s = 0.007$ (see Fig. 8b). Similarly, other periodic orbits can be found by varying the control parameter c_s . All these periodic orbits emerge via homoclinic explosions.

Fig. 8 Evolution of the flow trajectory of the intermittent-chaos (at $r = 166.1$) projected onto the X - Y plane (left) and the corresponding Poincaré map (right) for **a** $c_s = 0.005$, **b** $c_s = 0.007$

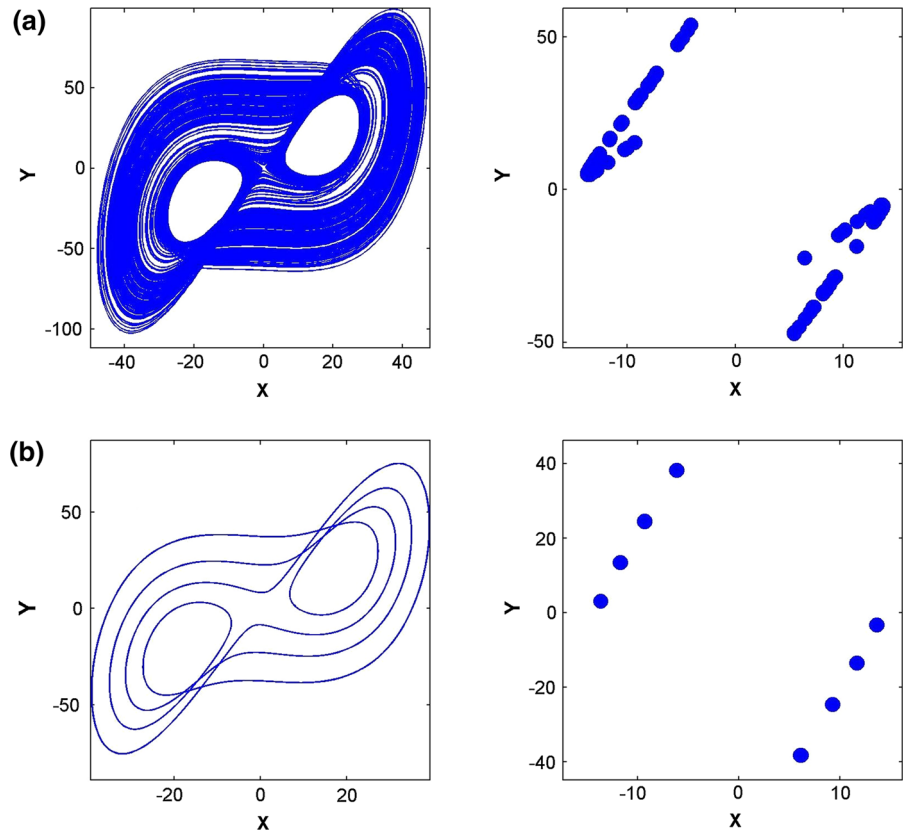


Fig. 9 Variation of **a** the Lyapunov exponents $\lambda_{1,2}$ and **b** the Kaplan–Yorke dimension D_{KY} with the couple-stress parameter c_s

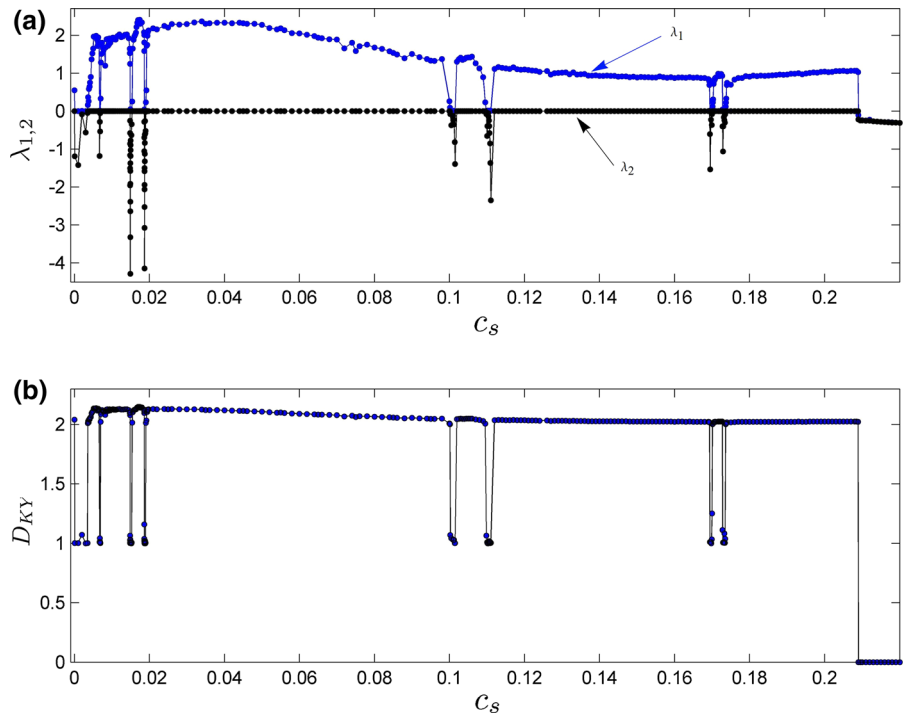
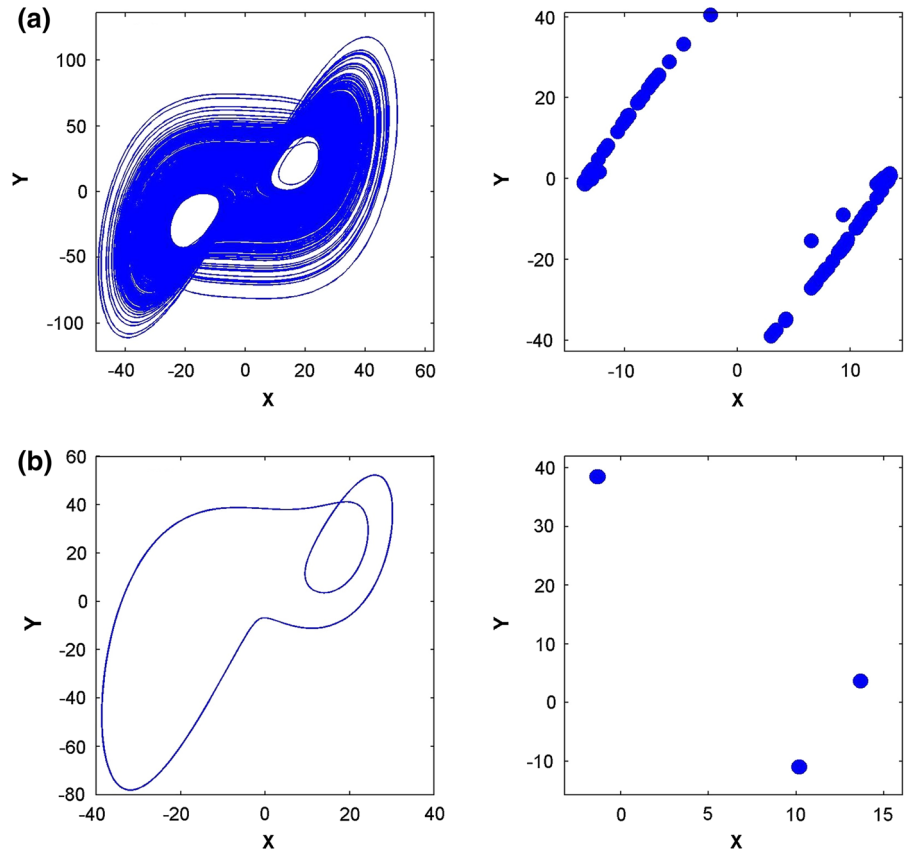


Fig. 10 Phase portrait of the intermittent-chaos(at $r = 166.1$) projected onto the X - Y plane (left) and the corresponding return map (right) for **a** $c_s = 0.012$, **b** $c_s = 0.01486$



A period-3 periodic orbit is obtained for $c_s = 0.01486$ (see Fig. 10b). Also, period-6 periodic solutions are found at $c_s = 0.101$ (see Fig. 11b), $c_s = 0.0186$, $c_s = 0.11003$, and $c_s = 0.174758$. Note that when c_s exceeds the value $c_s = 0.174758$, a chaotic solution emerges again. In this case, however, the return map contains no hook, as illustrated in Fig. 12 for $c_s = 0.2$.

An interesting result is obtained when c_s attains the value $c_s = 0.209802$. At this point, a semi-stable limit cycle emerges in the system which signifies a synchronization of the chaotic motion to a steady state. The projection of the limit cycle on the X - Y plane is presented in Fig. 13a. For further increase in c_s , the limit cycle disappears and the solution becomes steady for ever. The trajectory of the steady-state solution projected onto the X - Y plane is displayed in Fig. 13b for $c_s = 0.22$.

Finally, with increasing couple-stress parameter the synchronization of intermittent-chaos to a steady state takes place via a series of periodic motions interspersed with chaos. However, the chaotic solution of the system

at $r = 28$ below $c_s \approx 0.009$ directly synchronizes to a steady state.

7 Summary and concluding remarks

This is a study exploring the effects of particle size on thermo-convective motion of horizontal couple-stress fluid layer heated from below under a low-dimensional approach represented by Lorenz-like equations. The stability, local and global bifurcations, transition to chaos, intermittent-chaos, and synchronization to steady state are analyzed for this system. The main results are summarized below:

- (i) The equilibrium solution E_0 undergoes a supercritical pitchfork bifurcation when r reaches the critical value $r_p = c$, and for $r > r_p$, the solution E_0 becomes unstable and two non-trivial solutions E_{\pm} are born.
- (ii) The solutions E_{\pm} are stable as long as $r < r_h$, where $r_h = \sigma c^2(3 + b + c\sigma)/(c\sigma - b - 1)$, $\sigma > (1 + b)/c$. At $r = r_h$, the convective solutions E_{\pm}

Fig. 11 Phase trajectory of the intermittent-chaos (at $r = 166.1$) projected onto the X - Y plane (left) and the corresponding Poincaré section at $Z = 165$ (right) for the couple-stress parameter: **a** $c_s = 0.09$, **b** $c_s = 0.101$

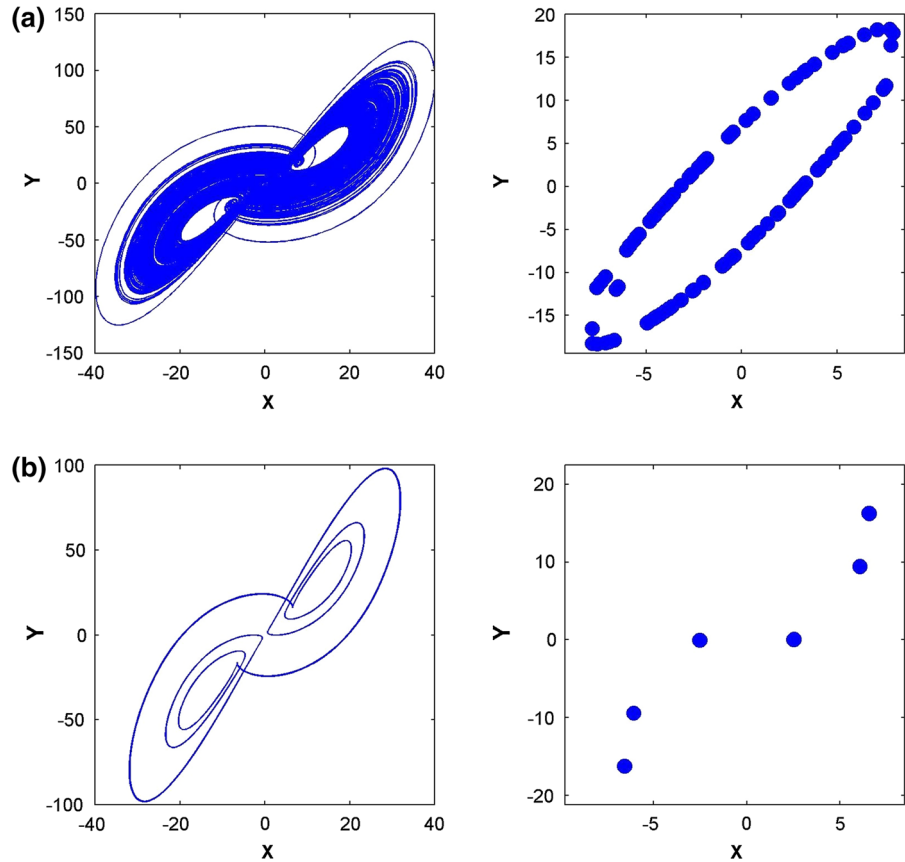
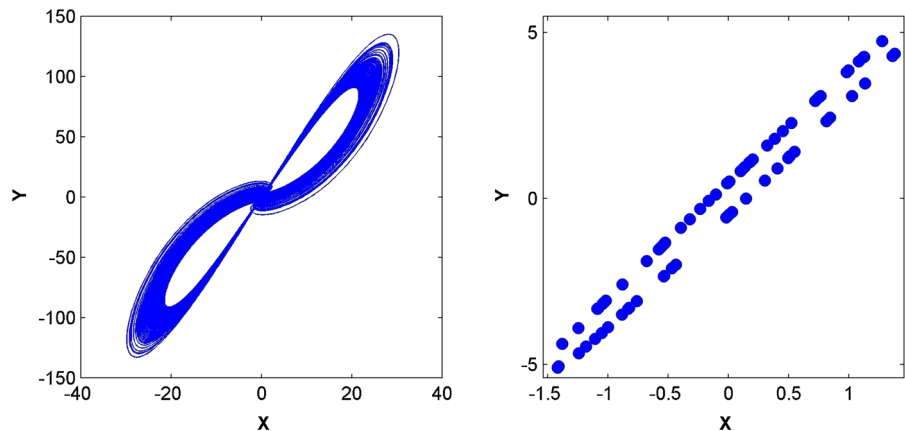


Fig. 12 Evolution of the flow trajectory of the intermittent-chaos (at $r = 166.1$) projected onto the X - Y plane (left) and the corresponding return map (right) for the couple-stress parameter $c_s = 0.2$

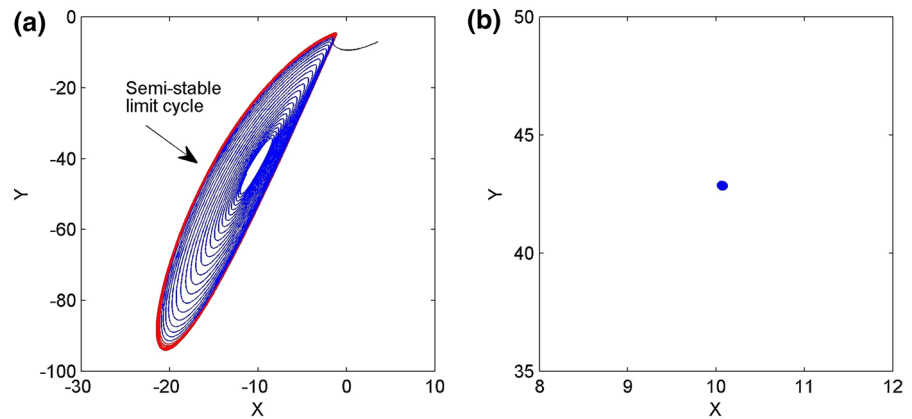


undergo a Hopf bifurcation, resulting a transition from stationary to oscillatory convection.

- (iii) Using first Lyapunov quantity, the Hopf bifurcation is of subcritical type. However, the hardness of the stability boundary at $r = r_h$ decreases with the couple-stress parameter c_s .

- (iv) For global aspects of dynamics of the nonlinear system (8) we found that between r_p and r_h there exists a critical normalized Rayleigh number, r_0 , where the system exhibits homoclinic loops connecting the origin with itself and the system undergoes a homoclinic bifurcation in the neighborhood of the origin.

Fig. 13 Phase trajectory at the final state at particular $r = 166.1$ projected onto the X - Y plane when **a** $c_s = 0.209802$, and **b** $c_s = 0.22$



- (v) Beyond r_0 , the trajectory wanders randomly around the equilibrium points E_{\pm} and decays eventually to either of them. The average time interval of wandering expands with increasing r , and finally, it becomes infinitely large when r attains another critical value $r_1 (< r_h)$.
- (vi) The synchronization of intermittent-chaos takes place via a series of periodic motion interspersed with intervals of chaotic behaviors. The saddle limit cycles are formed finally, and the system reaches the motionless conduction state.

Finally, the modeled system is useful in engineering transports such as heat transfer in fluids with long-chain molecules, melting and solidification of liquid crystals, polymeric suspension, lubrication technology, and bio-fluid transports.

Acknowledgements The authors would like to thank the Editor and anonymous Reviewers for their careful reading and constructive comments, which help a lot for improving the manuscript. One of the authors N. C. Pati (SRF) gratefully acknowledges the research Fellowship received from CSIR, New Delhi, India [No.: 09/025(0212)/2014-EMR-I].

References

1. Chandrasekhar, S.: Hydrodynamic and Hydromagnetic Stability. Oxford University Press, New York (1961)
2. Drazin, P.G., Reid, W.H.: Hydrodynamic Stability, 2nd edn. Cambridge University Press, Cambridge (2004)
3. Lorenz, E.N.: Deterministic nonperiodic flow. *J. Atmos. Sci.* **20**, 130–141 (1963)
4. Ramanaiah, G., Sarkar, P.: Slider bearings lubricated by fluids with couple stress. *Wear* **52**, 27–36 (1979)
5. Sinha, P., Singh, C.: Couple stresses in the lubrication of rolling contact bearings considering cavitation. *Wear* **67**, 85–98 (1981)

6. Gupta, R.S., Sharma, L.G.: Analysis of couple stress lubricant in hydrostatic thrust bearing. *Wear* **125**, 257–269 (1988)
7. Mokhiamer, U.M., Crosby, W.A., El-Gamal, H.A.: A study of a journal bearing lubricated by fluids with couple stress considering the elasticity of the liner. *Wear* **224**, 194–201 (1999)
8. Wang, X.L., Zhu, K.Q., Wen, S.Z.: On the performance of dynamically loaded journal bearings lubricated with couple stress fluids. *Tribol. Int.* **35**, 185–191 (2002)
9. El Shehawey, E.F., Mekheimer, K.S.: Couple-stresses in peristaltic transport of fluids. *J. Phys. D: Appl. Phys.* **27**, 1163 (1994)
10. Maiti, S., Misra, J.C.: Peristaltic transport of a couple stress fluid: some applications to hemodynamics. *J. Mech. Med. Biol.* **12**, 1250048 (2012)
11. Mekheimer, K.S.: Peristaltic transport of a couple-stress fluid in a uniform and non-uniform channels. *Biorheology* **39**, 755–765 (2002)
12. Mekheimer, K.S., Abd elmaboud, Y.: Peristaltic flow of a couple stress fluid in an annulus: application of an endoscope. *Physica A* **387**, 2403–2415 (2008)
13. Srivastava, L.M.: Flow of couple stress fluid through stenotic blood vessels. *J. Biomech.* **18**, 479–485 (1985)
14. Pralhad, R.N., Schultz, D.H.: Modeling of arterial stenosis and its applications to blood diseases. *Math. Biosci.* **190**, 203–220 (2004)
15. Eringen, A.C.: Simple microfluids. *Int. J. Eng. Sci.* **2**, 205–217 (1964)
16. Eringen, A.C.: Theory of micropolar fluids. *J. Math. Mech.* **16**, 1–18 (1966)
17. Bhattacharyya, K., Mukhopadhyay, S., Layek, G.C., Pop, I.: Effects of thermal radiation on micropolar fluid flow and heat transfer over a porous shrinking sheet. *Int. J. Heat Mass Transf.* **55**, 2945–2952 (2012)
18. Stokes, V.K.: Couple stresses in fluids. *Phys. Fluids* **9**, 1709–1715 (1966)
19. Ahmadi, G.: Stability of a cosserat fluid layer heated from below. *Acta Mech.* **31**, 243–252 (1979)
20. Banyal, A.S.: The necessary condition for the onset of stationary convection in couple-stress fluid. *Int. J. Fluid Mech. Res.* **38**, 450–457 (2011)
21. Sunil, R., Devi., Mahajan, A.: Global stability for thermal convection in a couple-stress fluid. *Int. Commun. Heat Mass Transf.* **38**, 938–942 (2011)

22. Jawdat, J.M., Hashim, I., Bhadauria, B.S., Momani, S.: Onset of chaotic convection in couple-stress fluids. *Math. Model. Anal.* **19**, 359–370 (2014)
23. Layek, G.C., Pati, N.C.: Bifurcations and chaos in convection taking non-Fourier heat-flux. *Phys. Lett. A* **381**, 3568–3575 (2017)
24. Wiggins, S.: *Introduction to Applied Nonlinear Dynamical Systems and Chaos*, vol. 2. Springer, New York (2003)
25. Layek, G.C.: *An Introduction to Dynamical Systems and Chaos*. Springer, India (2015)
26. Gang, H., Guo-jian, Y.: Instability in injected-laser and optical-bistable systems. *Phys. Rev. A* **38**, 1979 (1988)
27. Kuznetsov, Y.A.: *Elements of Applied Bifurcation Theory*, vol. 112, 3rd edn. Springer, New York (2004)
28. Hassard, B.D., Kazarinoff, N.D., Wan, Y.H.: *Theory and Applications of Hopf Bifurcation*. Cambridge University Press, Cambridge (1981)
29. Palis, J., Takens, F.: Hyperbolicity and the creation of homoclinic orbits. *Annals Math.* **125**, 337–374 (1987)
30. Sparrow, C.: *The Lorenz Equations: Bifurcations, Chaos, and Strange Attractors*. Springer, New York (1982)
31. Broer, H., Takens, F.: *Dynamical Systems and Chaos*. Springer, New York (2011)
32. Kaplan, J.L., Yorke, J.A.: Preturbulence: a regime observed in a fluid flow model of Lorenz. *Commun. Math. Phys.* **67**, 93–108 (1979)
33. Yorke, J.A., Yorke, E.D.: Metastable Chaos: the transition to sustained chaotic behavior in the Lorenz model. *J. Stat. Phys.* **21**, 263–277 (1979)
34. Bergé, P., Dubois, M., Manneville, P., Pomeau, Y.: Intermittency in Rayleigh-Bénard convection. *J. Phys. Lett.* **41**, 341–345 (1980)
35. Pomeau, Y., Manneville, P.: Intermittent transition to turbulence in dissipative dynamical systems. *Commun. Math. Phys.* **74**, 189–197 (1980)
36. Vadasz, P., Olek, S.: Weak turbulence and chaos for low Prandtl number gravity driven convection in porous media. *Trans. Porous Med.* **37**, 69–91 (1999)
37. Wolf, A., Swift, J.B., Swinney, H.L., Vastano, J.A.: Determining Lyapunov exponents from a time series. *Physica D* **16**, 285–317 (1985)
38. Kaplan, J.L., Yorke, J.A.: Chaotic behavior of multidimensional difference equations. In: Peitgen, H.O., Walthers, H.O. (eds.) *Functional Differential Equations and Approximation of Fixed Points Lecture Notes in Mathematics*, vol. 730, pp. 204–227. Springer, Berlin (1979)